Numerical model for sparking and plasma formation during spark plasma sintering of ceramic compacts

Rachel Marder, Claude Estournès, Geoffroy Chevallier, Rachman Chaim

Numerical model for sparking and plasma formation during spark plasma sintering of ceramic compacts

R. Marder[1] · C. Estournès[2,3] · G. Chevallier[2,3] · R. Chaim[1]

Abstract The conditions for spark discharge and plasma formation in non-conducting ceramic granular compacts subjected to spark plasma sintering (SPS) were analyzed. The SPS plungers-die-powder assembly was modeled, whereby a compact of spherical YAG nanoparticles was considered. Electric resistance of the simulated SPS assembly versus temperature was comparable to that of the experimental SPS system. The conditions for particle surface charging and discharge were determined with respect to the applied current, the SPS temperature, and duration. Sudden increase in the electric current through the simulated granular compact was observed around 1200 °C, confirming the percolative nature of the current. This finding is in agreement with the experimental densification start at 1250 °C. Moreover, the electric current percolation was simulated by passing a DC current through a modeled granular compact box, comprised of resistors and capacitors which resembled the particle's surface resistivity and the inter-particle gaps, respectively. Spark discharge and plasma formation depend on connectivity within the granular compact and cease with the formation of a close-packed system.

✉ R. Marder
rachelma@technion.ac.il

[1] Department of Materials Science and Engineering, Technion – Israel Institute of Technology, 32000 Haifa, Israel

[2] UPS, INP, Institut Carnot Cirimat, Université de Toulouse, 118, route de Narbonne, 31062 Toulouse Cedex 9, France

[3] CNRS, Institut Carnot Cirimat, 31062 Toulouse, France

Introduction

During the Spark Plasma Sintering (SPS) process, a pulsed DC current is directly applied to the die-powder assembly, resembling superfast heated hot-pressing conditions. The electric current which is forced to flow through the die-powder-assembly results in resistance heating, leading to the densification and sintering of the powder compact. The SPS process can be applied to metallic as well as to ceramic powder compacts; however, the manner the current flows through the powder-die assembly strongly depends on the electric conductivities of the powder and the surrounding die. Previous thermal-electrical model simulations have shown that for insulating powders almost all the current flew through the conductive graphite die [1–4]. In the case of oxides, only a small current portion is believed to flow through the dielectric powders. Gurt-Santanach et al. have shown that sintering a reactive alumina–hematite solid solution (far less conducting than graphite at room temperature), while changing the pulse pattern for a given sintering cycle, modifies the current crest intensities and has a great influence on the microstructure [5]. However, the electrical bulk conductivity of several ceramics increases by several orders of magnitude during the heating. For example, the electrical conductivity of YAG increases from 10^{-14} S·cm^{-1} at 400 °C to 10^{-6} S·cm^{-1} at 1000 °C [6]. Therefore, at some temperature during the heating, the electrical conductivity of the ceramic dielectric becomes high enough and comparable to the conductivity of the graphite die. At this temperature, percolation of the electric current through the ceramic granular compact starts. The electric current flow through the granular compact may eventually lead to discharges at the gaps between particles, occasionally accompanied by spark and plasma formation [7–13]. Nevertheless, the concept about

the negligible current through the dielectric powder compacts did not promote further investigations of the current effects in such granular systems subjected to SPS.

However, whether plasma is formed or not depends on several conditions, one of them is the ability of the powder to undergo plastic deformation. Recently, plastic yield–plasma formation windows diagrams were introduced with respect to the SPS process [7–9]. These diagrams (i.e., Fig. 1) are based on the electrical conductivity and the plastic yield of the material and their changes with the temperature; they also show the temperature windows for plastic deformation and for plasma formation. One requirement for the plasma formation is a non-continuous material network; voids in the compact allow the necessary conditions for surface charging and discharges between the particles. Thus, materials with low yield strength, which undergo plastic deformation, lack the plasma effect, since the applied pressure in SPS transforms the loose powder compact to a continuous network. Another requirement for plasma formation is that the surface electric conductivity has to be high enough so that current percolation can take place. This critical electrical conductivity value was chosen between 10^{-9} and 10^{-5} S·cm^{-1} as the threshold values for the current percolation [7], and is based on Takuma and coworkers' theoretical calculations [14, 15]. They calculated the intensification of the electric field around dielectric objects, and found that the applied electric field can be intensified by 2–3 orders of magnitude, close to the contact points between neighboring objects, for resistivity between 10^6 and 10^7 Ω·cm. At these conditions, the isolating compact behaves as a conductor, i.e., the current percolates through the compact.

The discussion whether plasma is formed or not formed during the SPS process is long lasting. Tokita [16] was among the first in the early 90s to explain the formation of plasma during SPS of metallic powders. Nevertheless, the presence of plasma during the SPS of non-conductive

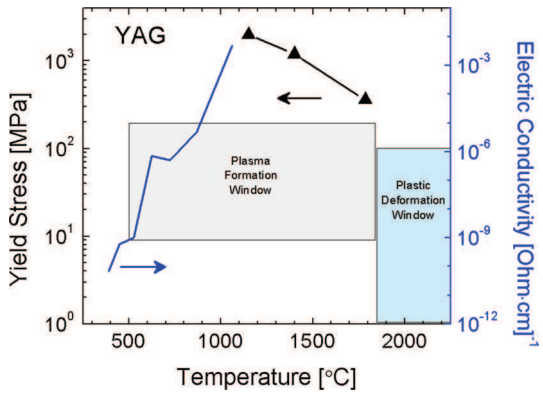

Fig. 1 Plastic deformation—plasma formation windows diagram for nc-YAG subjected to SPS at 100 MPa (Ref. [9])

powders is under debate. Recently, several publications addressed the aspect of plasma formation in non-conductive ceramics [7–9, 12, 13]; these works presented microstructural features, such as material jets, and explained their structures by the existence of spark and plasma.

The present work addresses the aspect of plasma formation during the SPS of ceramic powders. It presents an analysis of the electric current through the SPS system, and the granular ceramic in particular. The conditions for surface breakdown and plasma formation are discussed. Finally, a 2D Matlab model is presented for understanding the electric current percolation in the ceramic powder compact.

Experimental procedure and modeling

The present analysis is based on Yttrium Aluminum Garnet (YAG) specimens which were produced by SPS under uniaxial pressure of 100 MPa from 600 °C to different final temperatures, ranging from 1100 to 1400 °C. Pure commercial nanocrystalline (nc) YAG powder (Nanocerox, USA) with spherical morphology and a mean crystallite size (diameter) of 70 ± 50 nm was used. Disks of 8 mm in diameter were fabricated. The detailed description of the experimental SPS conditions, the densification, and the observed microstructures were described elsewhere [9].

The SPS system used was a Dr. Sinter 2080 SPS apparatus, located at the Plateforme Nationale CNRS de Frittage Flash (PNF2/CNRS) at Université Toulouse 3 Paul Sabatier, France. Figure 2 shows a schematic of the SPS system with the different die and plunger components, including the geometrical dimensions. The die, punches, and spacers were made of graphite (Mersen reference 2333), while the Ram Cover is Inconel 600. A heating rate of 100 °C·min^{-1} was used, which is comparable to the maximum current density of 100 A·cm^{-2}. The voltage–current conditions used included DC-pulse duration of 3.3 ms with pulse sequences 12-2 (12 pulses ON followed by 2 dead times—pulse OFF). Voltage, current, temperature, pressure, and ram displacement were recorded during the process.

Matlab was used to model the electric current percolation through the granular non-conducting oxide (YAG) during the SPS. A two-dimensional (2D) box with randomly distributed circular disks (corresponding to spherical particles in three dimensions) with log-normal size distribution was constructed. The 2D box dimensions are as presented in Fig. 3a. The box consisted of more than 600 particles with an average particle diameter of 70 nm. The box was first filled with mono-sized disks in ordered close-packed conditions, then a small amount of circles were removed, and the remaining circles were allowed to

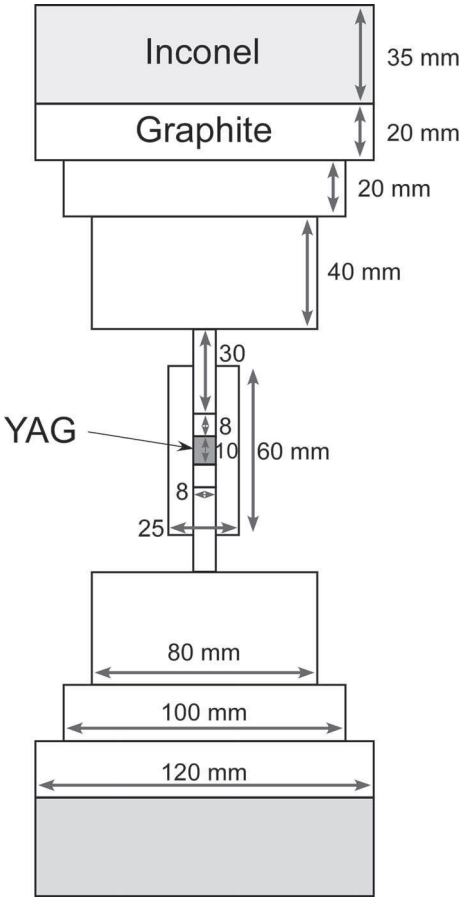

Fig. 2 SPS set-up showing die and plunger elements

rearrange until they reached a random loose-packed state. A log-normal particle size distribution was achieved by allowing the radius of the disks to grow or shrink (within a certain limit) during the rearrangement iterations. The resultant particle size distribution is presented in Fig. 3b. The packing density (relative density) of the box, filled with disks with log-normal diameter distribution, was finally set around 74 %, close to the reported random loose-packing (RLP) for 2D [17]. The "shortest path algorithm" [18] was used to model the electric current percolation through the powder compact.

Results and discussion

Analysis of electric current through SPS system

The change in density of the YAG compact during the SPS heating to 1400 °C at 100 MPa pressure is shown in Fig. 4; the figure includes the voltage and the current recorded during the process versus the temperature. The densification starts around 900 °C, stagnates between 1060 and 1200 °C, and reaches its maximal rate at 1380 °C. A phase-transformation taking place during the heating attributed to this shrinkage stagnation [9]. The voltage and current increased during the SPS heating from approximately 3 to 6 V and from ~300 to ~800 A, respectively. The changes in voltage and current are proportional as expected from Ohm's law; the SPS system has an essentially resistive behavior as mentioned above and previously reported [19]. At 750 °C, the voltage-current of the system stabilizes and the voltage and current increase linearly above this temperature.

The recorded current is the average electric current that flows through the whole SPS system during the process. Of particular interest is the current that passes through the powder compact, since the densification mechanism in SPS is strongly connected to the electric current and electric field effects in the powder during the sintering process. The electric current through the YAG nanopowder compact was

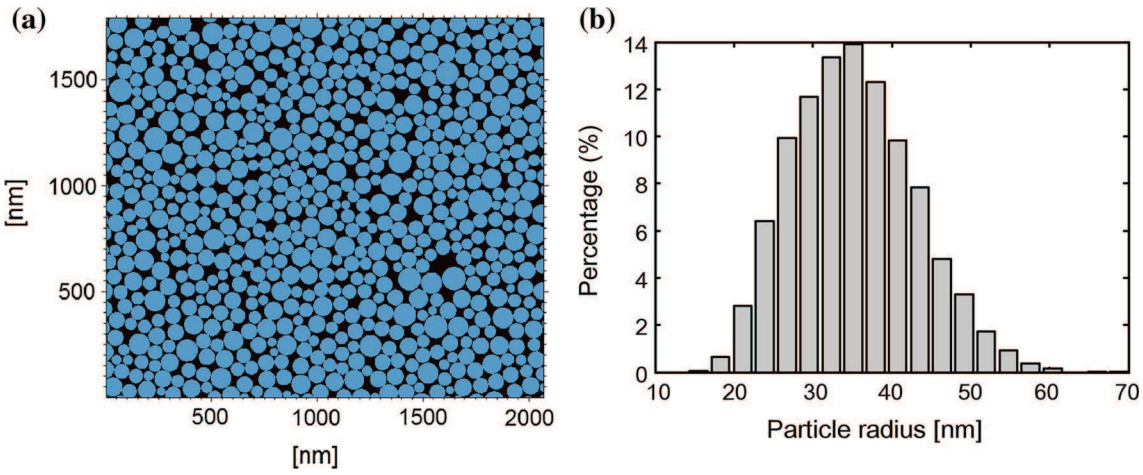

Fig. 3 **a** 2D box with circular particles in a random loose-packed arrangement, **b** log-normal particle radius distribution in the 2D box. The modeled resultant density of the box in **a** is 0.735 ± 0.02 with a mean particles radius **b** of 35.2 ± 7.4 nm

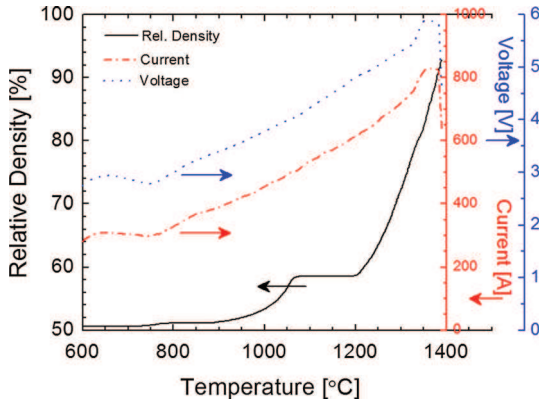

Fig. 4 SPS profile for YAG nanopowder compact heated from 600 to 1400 °C under 100 MPa showing the density (*black solid*), voltage (*blue dotted*), and current (*red dot-dashed*) changes versus temperature (Color figure online)

estimated by modeling the SPS system and considering the electric resistance of each component. The SPS configuration used in the present work is similar to that presented in [19, 20]; the same SPS apparatus used to model the thermal conductivity of the system. The modeled SPS system consists of a graphite die, the powder, and several graphite and metallic (Inconel 600) plunger elements. The resistance of the graphite and the Inconel parts were calculated using Eq. (1):

$$R = \rho \times \frac{l}{A}, \tag{1}$$

where ρ is the resistivity of the component's material, l is the height of the component along the electric current direction, and A the surface perpendicular to the electric current flow. The dimensions of the different elements can be seen in Fig. 2. The electrical resistivities of graphite and Inconel were taken from Ref. [20]. The powder and the surrounding graphite die can be treated as two parallel resistors, which are in turn connected in series with the graphite and Inconel plungers. The electric resistance of the granular powder was estimated using the approach explained in [21], where the granular powder is compared to an assembly of particle chains whose lengths depend on a characteristic electric current path, and which in turn, is a function of the relative powder density (D). The average length of one particle chain (L) can be written as [21]

$$L = D^{\frac{1-m}{2}} \times h, \tag{2}$$

where m is a constant factor (between 1.8 and 2) and h is the height of the powder compact. The electric resistance of one conductive chain (R_{chain}) is equivalent to the sum of the contact resistances of the touching particles within the chain, similar to resistors connected in series, and can be calculated by

$$R_{\text{chain}} = \frac{2}{Z} \times R_{\text{c}} \times N_{\text{p}}, \tag{3}$$

where Z is the coordination number (depends on the compact density), R_{c} is the contact resistance between two touching particles, and N_{p} is the average number of powder particles in one chain. N_{p} can be calculated using the particle radius (r):

$$N_{\text{p}} = \frac{L}{1.5 \times r}. \tag{4}$$

For simplification, mono-sized spherical particles with a diameter of 100 nm were considered. The contact resistance between two particles (R_{c}) is [22]

$$R_{\text{c}} = \frac{\rho}{2 \times r_{\text{a}}}, \tag{5}$$

where ρ is the electrical bulk resistivity of the powder material (i.e., YAG) and r_{a} is the contact area radius between particles. The contact area is the Hertzian contact and is a function of the applied pressure and the particle material properties, such as elastic modulus (E) and Poisson's ratio (ν):

$$r_{\text{a}} = \left[\frac{3 \times (1 - \nu^2)}{4 \times E} \times r \times f\right]^{\frac{1}{3}} \tag{6}$$

where f is the effective load on each particle, calculated from the applied pressure. Finally, the resistance of the granular compact is calculated as follows:

$$R_{\text{powder}} = \frac{R_{\text{chain}}}{N_{\text{chains}}}, \tag{7}$$

where N_{chains} is the number of conductive particle chains, calculated by dividing the total number of particles to the number of particles per chain, assuming that each particle belongs to one particular chain. The total number of particles in the powder is calculated using the green compact volume, which has a diameter of 8 mm and a height of approximately 10 mm. In order to calculate the resistance of the powder compact, the electrical bulk resistivity of YAG was estimated from [6], by fitting the logarithm of the electrical conductivity to a polynomial curve (with $R = 0.973$). A granular relative density of 0.60 was assumed, which is close to the relative density (D) of the compacted powder, prior to reaching the highest shrinkage rate (see Fig. 4). Finally, the particle coordination number was calculated according to [23]

$$Z = 2 + 11 \times D^2. \tag{8}$$

The final resistance of the SPS set-up was calculated using Eqs. (1) through (8), and the laws of series and parallel circuits. Ideal contacts between the SPS set-up components were assumed, disregarding possible contact resistances.

This is justified considering the fact that for SPS at high pressures (i.e., 50 MPa and higher), the contact resistances are low and negligible [24]. The electrical resistivity values used for YAG, graphite, and Inconel are summarized in Table 1. The calculated electrical resistance of the entire SPS system versus temperature is presented in Fig. 5a by the dashed blue curve. The calculated electrical resistance at 700 °C is close to 9.6 mΩ and decreases to 7.5 mΩ at 1400 °C.

In order to justify the calculated value, the electrical resistance of the SPS system was calculated as well, using the recorded data during the SPS process. The resistance can be calculated as a function of applied voltage and current, according to Ohm's law:

$$R = \frac{V}{I}, \tag{9}$$

where I and V are the recorded current and voltage during the SPS experiment, respectively. Figure 5a shows the extracted resistance from the recorded data (solid red curve) together with the modeled resistance according to the SPS components (dashed blue curve). The modeled value showed good correlation to the experimental value (extracted from the SPS data), which substantiates the calculations for the modeled electrical resistance.

Figure 5b shows the calculated electric currents through the entire SPS system (dotted blue curve) and through the powder compact (solid red curve). The currents were calculated for a linearly increasing voltage from 3 to 6 V between 700 and 1400 °C, to consider the voltage increase during the SPS process, as it can be seen by the recorded data (dotted blue curve in Fig. 4). The recorded current, as measured by the SPS apparatus, was added for comparison to Fig. 5b (dot-dashed gray curve). The current through the granular compact and through the die-plungers assembly was calculated according to Ohm's law and by using the respective calculated resistances discussed above. As expected for bad conductors at low temperatures, such as YAG, almost all the current flows through the graphite die. However, logarithmic increase in the current through the compact was observed at ~1200 °C, as shown by the insert in Fig. 5b. This current increment can be explained by the fact that the electrical conductivity of YAG increases by several orders of magnitude with the increasing temperature. At some critical temperature (T_{crit}), the electrical resistivity of the powder reaches the magnitude similar to that of graphite. At this point, the electric current will start to flow through the powder compact as well.

Many particles are in real contacts with other particles, while some parts of the particles face toward cavities, or are in close proximity with neighbor particles, without contact. Therefore, once the compact reaches the appropriate electrical conductivity, percolation of the current takes place via the particle surfaces and through the contacts, simultaneously charging the particles at the gaps. Once the percolation is completed along the compact height, no further charging is expected. Close to T_{crit} the particles start to conduct electric current, preferably along their surfaces, since the resistivity of the dielectric surfaces is lower than the bulk resistivity. At this stage, the DC-pulsed nature of the current with very high current density (i.e., 100 A·cm^{-2}) forces accumulation of the charge at the particle surfaces, particularly at the surfaces with gaps between neighboring particles. Such a pair of particles with the small gap in between, acts as a small capacitor with gas/air as dielectric medium between its charged surfaces. In general, the powder is compared to an array of resistor elements (particles) together with small capacitors (gaps). The charge accumulation may increase in such a way that the local potential at the gap reaches the breakdown voltage of the gas/air in the gap [25] or fulfilling the conditions for field emission at the YAG surface. This would eventually lead to discharges across the gap, resulting in three different effects: (a) sparking from the charged surface to the closest non-charged surface over the gap, associated with a jet of molten material removed from the charge surface; (b) sparking and transfer of high density of electrons to the opposite non-charged particle surface and its local melting; and (c) sparking and ionization of the existing gas residues and molecules at the gap, by the ejected electrons from the charge surface, hence the formation of plasma and its spread over the other cavities and larger volumes. Once a jet of material was formed or plasma was evolved, the gap is electrically and temporarily short circuited and converts to a resistor element. Recently, such

Table 1 Electrical bulk resistivity ρ of graphite, Inconel, and YAG

Material	Electrical bulk resistivity (Ω·m)	Reference
YAG	$\log\left(\frac{1}{\rho}\right) = 2.18 \times 10^2 - 6.19 \times 10^5 \times T^{-1} + 5.63 \times 10^8 \times T^{-2} - 1.72 \times 10^{11} \times T^{-3}$	Calculated with data from [6]
Graphite	$\rho = 2.14 \times 10^{-5} - 1.34 \times 10^{-8} \times T + 4.42 \times 10^{-12} \times T^2$	[20]
Inconel 600	$\rho = 9.82 \times 10^{-7} - 1.6 \times 10^{-10} \times T$	[20]

T is the temperature in (K)

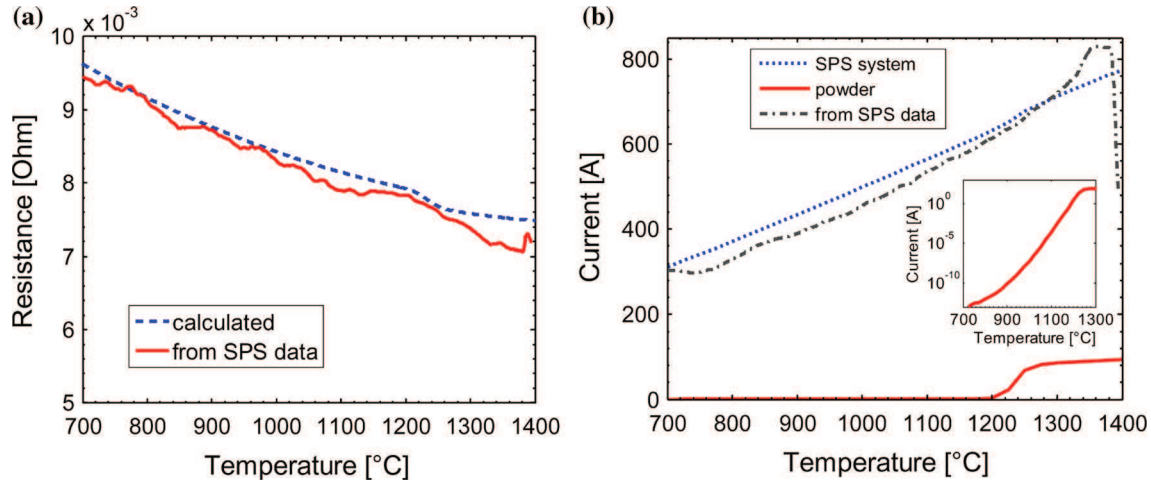

Fig. 5 **a** Modeled electric resistance (*dashed blue curve*) and experimental electric resistance of the SPS assembly (*solid red curve*) versus temperature. **b** Calculated electric current through the SPS assembly (*dotted blue curve*) and through the powder compact (*solid red curve*), and recorded current, as measured by the SPS apparatus (*dot-dashed gray curve*) during SPS. The *insert* is a magnification of the current through the powder compact (Color figure online)

jet-like necks connecting between adjacent particles over the gaps between them were found in YAG granular compacts after heating by SPS to 1200 °C, and were presented in a previous paper [9]. The existence of such jet-like necks sustains the scenario explained above, in which sparking and plasma take place at the gaps between particles in a granular compact during the SPS process.

For spark and finally plasma to occur, a minimal critical amount of electric charges has to be present at the particle surfaces facing the gaps, otherwise no electrical discharges will occur. For air/gas breakdown in the small gaps between particles, the charge accumulated due to the electric voltage/current has to be at least in the order of the breakdown voltage of air (V_{bd}). The amount of charge (Q_A) which accumulates in average at the particles surfaces of the entire compact due to the applied pulsed DC is estimated by

$$Q_A = I \times t, \tag{10}$$

where I is the electric current through the granular compact at T_{crit} and t is the time. The average charge density (q_A) at the particle surfaces is approximately

$$q_A = \frac{Q_A}{A_{eff}}, \tag{11}$$

where A_{eff} is average surface area of the compact, estimated by multiplying the surface area of one particle with the approximate number of the particles, and subtracting the particle contact areas, while considering the average coordination number. We assume that the contact area is much smaller than the particle surface area. However, the charge density calculated according to Eq. (11) is an average value, and locally, much higher charge densities may develop.

The breakdown voltage (dielectric strength) of air is considered to be in the order of 3×10^6 V/m; however, this value may increase for small gaps, and therefore, the more conservative value of 3×10^8 V/m was also considered in the present analysis. Since the particles facing the small gaps are considered as small capacitors, the critical charge needed for breakdown (Q_{bd}) is estimated by

$$Q_{bd} = C \times V \times \left[1 - \exp\left(-\frac{t}{RC}\right)\right] \tag{12}$$

where R is the resistance of the capacitor and C is its capacitance. The small capacitor assumed as two-sphere capacitor, with its capacitance according to Lekner [26]

$$C = 2 \times \pi \times \varepsilon_0 \times r \times \left(\log(2) + 0.57721 - \frac{1}{2} \times \log\left(\frac{2 \times r + g}{r} - 2\right)\right), \tag{13}$$

where r is the particle radius and g the gap length which was assumed to be between 20 and 100 nm. The exponential in Eq. (12) tends to be very small for any reasonable resistance and time, in the range between a few milliseconds (one pulse) to a few minutes (the total SPS time). Therefore, simplification of Eq. (12) by assuming $Q_{bd} \approx C \cdot V$ is justified. The average surface charge density needed for breakdown according to the dielectric strength of air is estimated as the critical charge Q_{bd} divided by the capacitors surface (i.e., area of two half-spheres):

$$q_{bd} = \frac{Q_{bd}}{4\pi r^2} \tag{14}$$

The surface charge densities, calculated according to the applied current (q_A), and according to the breakdown

voltage (q_{bd}), are compared in Fig. 6. The plot shows that the charge density accumulated in average at the particle surface (blue solid curve) reaches the value needed for breakdown between 1150 and 1190 °C. These temperatures are close to 1225 °C, the temperature at which a logarithmic increase in the powder compact conductivity ceased (Fig. 5b). Moreover, it is interesting to note that this temperature is close to the temperature where jet-like necks between YAG grains are found in the sintered microstructure (1200 °C) [9]. Therefore, the present SPS model for granular ceramics strengthens the findings presented in [9], where formation of the jet-like necks is explained by plasma formation and supported by the plasma formation–plastic deformation diagrams.

The results of the simplified charge density calculations shown above, may not be taken as absolute values, but rather represent average values that may certainly be expected. Locally, much higher charge densities can build up due to our conservative approach. The possibility for sparking and plasma formation at these loci is higher and should occur at lower temperatures. Generally, the present analysis shows that enough charge needed for spark and discharges exists at the particle surfaces. It follows that the gaps between the particles play a significant role in the plasma formation, and represent the critical loci where discharges take place. Therefore, the residual evidences for plasma found, such as the jet-like 'grains' in YAG [9] and in LiF [8], were located at the cavities between the particles/grains, in addition to the locally solidified liquid droplets between the LiF grains.

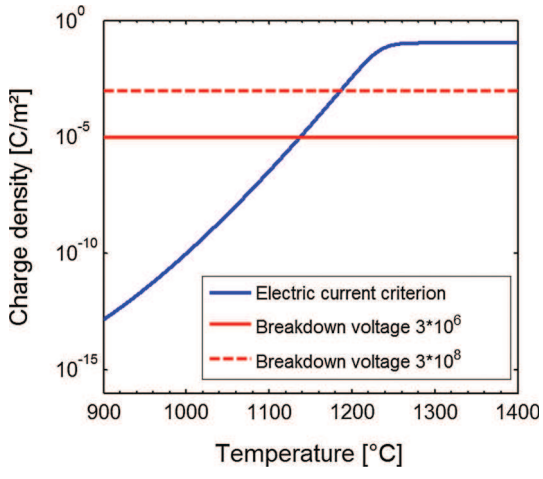

Fig. 6 Surface charge density calculated according to breakdown voltage conditions for two different breakdown voltage values (*red solid* and *dashed lines*) and surface charge density calculated from the electric current through the powder compact (*blue solid curve*) during SPS at 3 V. The charge density was calculated for charge accumulated at a time of one DC-pulse duration (0.04 ms) (Color figure online)

Current percolation in granular compact

The ceramic powder in the die, prior to sintering, is an array of bad-conducting elements. The array consists of contacting and non-contacting particles, hence is discontinuous; eventually small gaps between the particles are present. A non-continuous particle array was designed in 2D in Matlab (Fig. 3), in order to model the electric current percolation through the powder during SPS. In the 2D box built with the circular particles (Fig. 7), the top of the box represents one electrode. A voltage drop over the box height is caused by the non-conducting nature of the particles. At the beginning of the SPS process, no current is expected in the ceramic compact, due to its low conductivity. However, as explained above, when reaching the critical temperature T_{crit} during the heating, the powder starts to conduct (its electrical resistivity is similar to the graphite die), implying that electric current starts to flow at the particle surfaces. The current flow was modeled by assuming its start at the top of the box, and the flow forwards the bottom of the box, as much as possible in parallel to the direction of the electric field (voltage gradient). However, the existing gaps between the particles may block the current passage, terminating a current path, implying that no current flows through the void across the gap. In that case, the electric charge is accumulated and a capacitor between the last particle and the surrounding particles is built. Therefore, the box is made of resistors which represent the conducting passes between particles, or between a particle and the electrode, and of capacitors which are the gaps between two conducting passes.

In order to assure surface conduction in the model, the current was allowed to flow along the particle circumferences, but not through the particle itself. This was done by defining different 'costs' for steps of the advancing electric current on different paths: the step costs were low near the circumference and infinitely high inside the particles. Moreover, discharges at the gaps can occur, and the electric current can pass from one particle surface facing the gap directly through the void, and to the next particle facing the gap. Therefore, an additional cost was set for these direct jumps through the gaps between neighboring particles. Finally, the simulated current path was a combination of the shortest path and the path with the lowest total costs. Jumps occurred only in cases where the 'price' for jumping from one particle to the other was lower than the cost for advancing along one particle circumference. Thus, the defined 'cost' is directly related to the electric conductivity of the powder. For example, in the case of a good conductor, the cost for jumps between particles should be relatively high, assuring that the electric current flows almost only along the particle circumferences, even if the chosen path is much longer. On the other hand, for bad

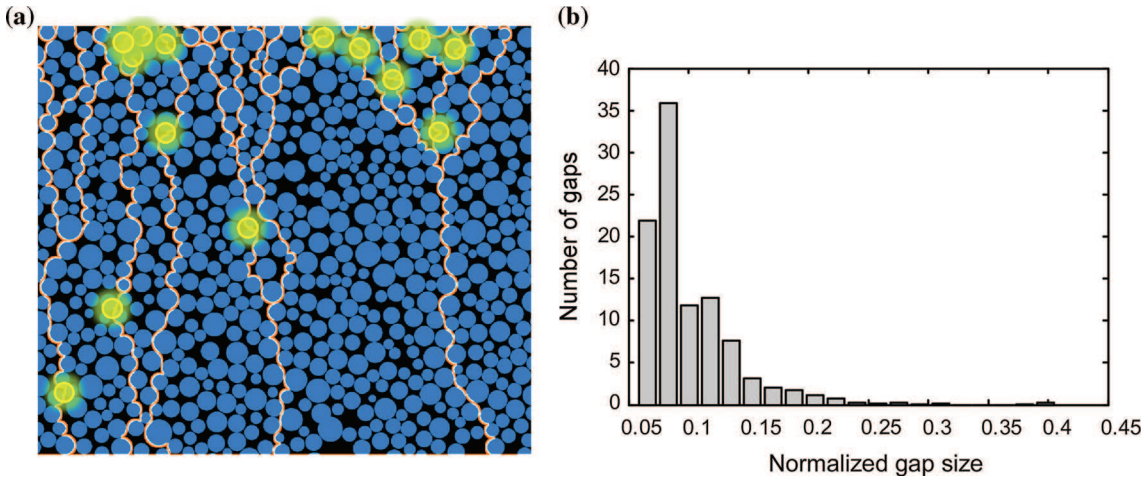

Fig. 7 **a** Simulation of current percolation in a 2D particle box showing current flow paths (*red*) and current discharges (*yellow circles*) during the flow. **b** Histogram showing the number of discharges found after five iterations as a function of the normalized gap size (Color figure online)

conductors, a lower price for jumps should be set, so that the electric current jumps across the gap occurred more often (compared to the case of a good conductor). It was noticed, after several simulations of the electric current flow with different jump-costs, that the change from the conductor to the non-conductor case occurred suddenly, i.e., a sharp transition exists from the case where no jumps were detected to the case where a high number of jumps were detected. This critical cost was selected for the model as the percolation threshold for the value of the jumps, since the ceramic acts first as non-conductor and changes its character with the heating to semi-conductor and conductor.

Figure 7a shows the particle box with the simulated current flow for one simulation cycle, showing its percolative character. During the electric current flow, several current discharges were noticed (marked with circles in Fig. 7a). Only the large gaps were selected (of 15 nm and above), since small gaps are insignificant, as discharges cannot occur in small gaps due to lack of accumulated charge. It is visible, that for a given electric flow path, a few gaps are present. Moreover, these critical locations for discharges and plasma are present throughout the compact. Figure 7b shows the statistics of the number of discharges taken from five simulations, as a function of normalized gap size (i.e., the gap distance divided by the particle size). Most of the discharges occur in relatively small gaps (smaller than 10 nm); however, a few discharges in larger gaps were found, which are of interest, since plasma can form in the larger gaps.

Discharges occur as long as the small capacitors are built up, and charge is accumulated. Once the electric flow founds a conductive path from the top to the box's bottom, the electric circuit is closed and no discharges will occur. That is, the current percolation ends. However, due to the pulsed nature of the current, the flow can start from different locations at each pulse, and charge can be accumulated at several points with the time, increasing the possibilities for discharges in the granular compact. Due to the percolative nature of the transport properties (i.e., electrical conductivity), the condition (and time) at which these discharge events (and eventually plasma) end is determined by the percolation limit, for 2D system: i.e., $pc = 0.5$ (for 3D system $pc = 0.17$). This means that once 50 % of the gaps (small capacitors) were active and caused to discharge, the current has passed along the box (from the top to the bottom) and the short circuit is reached. With the increase in density, the amount of free spaces in the powder decreases. The gaps get smaller and their number decreases. Moreover, the overall continuity of the compact is of great importance, since the charging–discharging scenario is limited by the percolation limit. Once the percolation is complete along the box height, no further charging is expected. Consequently, the time frame for particle charge–discharge is between the current percolation start and ending within the compact. The probability for plasma formation significantly decreases at high relative densities. Plasma formation is therefore constrained by the temperature, which defines the electric conductivity and by the applied pressure which sets the packing density, and the compact continuity.

The given model presents the 2D condition. Yet, the relation of the present model to the 3D situation, which describes more precisely a real powder compact, will be discussed briefly. The coordination number of 3–4 in 2D increases to 6–7 in 3D for a relative packing density of ~ 0.6, with the consequence, that the discharge probability increases by a factor of ~ 2 due to this dimensional transformation. The number of the efficient current paths increases, by moving from 2D to 3D (at a given packing

density). Nevertheless, the plasma events directly depend on the gap presence rather than the efficient current paths. Eventually, during densification, efficient current paths will form; however, no plasma is expected in the lack of gaps. Consequently, the gap number density increases by moving from 2D to 3D, which, in turn, increases the probability for occurrence of plasma events when reaching the percolation threshold. Moreover, the 2D percolation threshold is 0.5 where that of 3D is 0.17. This leads to the multiplication factor of $0.5/0.17 = 2.94$, which indicates that current percolation threshold can be attained at much easier conditions, i.e., at lower green densities.

An additional factor which can increase the discharge probability is the time response of the simulation model. The time response of the granular box is set by the optimal 'cost' of the discharge event. However, in reality and within the framework of the physical systems, the time response of the powder compact to the passing pulsed current is much shorter, i.e., at a given time, more paths exist for the current flow. These unexpressed paths for the charging and recharging processes may contribute to higher density of discharge events at a given time interval. Moreover, the simulation represents the electric current flow for a static powder state. However, during densification at low densities, the particles are constantly in motion, and even the smallest changes in the particle configuration create new contacts and current paths, to increase the possibilities for discharges and plasma formation.

Summary and conclusions

The presence of spark and plasma in SPS densification of non-conducting materials has been the subject of debate these last years. Recent works have evidenced the presence of molten jets of materials (YAG, LiF etc.) far below their melting temperatures, which can be the signature of such phenomenon. In the present paper, YAG specimens were produced by SPS under uniaxial pressure of 100 MPa from 600 °C to different final temperatures, ranging from 1100 to 1400 °C. The electric current through the YAG nanopowder compact was estimated by modeling the SPS system and considering the electric resistance of each component. The YAG granular powder compared to a compact box containing an assembly of particle chains, where depending of the SPS temperature, a fraction of the total DC current goes through. Then, the electric current percolation simulated considering the electric resistance of the conductive chains comprised of resistors (particles) and capacitors (gaps between the particles) which resembled the particle's surface resistivity and the inter-particle gaps, respectively. Considering this model, the conditions for particle surface charging and discharge were determined with respect to the applied current, the SPS temperature, and duration. It clearly showed that spark discharge and plasma may occur and their formation depend on connectivity within the granular compact and cease with the formation of a close-packed system. The average charge density accumulated at the particle surfaces reaches the value needed for breakdown between 1150 and 1190 °C, the temperature range where jet-like necks between YAG grains found in the sintered microstructure (1200 °C).

Acknowledgements R. Marder acknowledges the support of the fellowship from the Women in Science program of the Israel Ministry of Science and Technology.

References

1. Guillon O, Gonzalez-Julian J, Dargatz B, Kessel T, Schierning G, Rathel J, Herrmann M (2014) Field-assisted sintering technology/spark plasma sintering: mechanisms, materials, and technology developments. Adv Eng Mater 16:830–849
2. McWilliams B, Yu J, Zavaliagos A (2015) Fully couples thermal-electric simulation of electric field assisted sintering of net-shape compacts. J Mater Sci 50:519–530. doi:10.1007/s10853-014-8463-1
3. Anselmi-Tamburini U, Gennari S, Garay JE, Munir ZA (2005) Fundamental investigations on the spark plasma sintering/synthesis process II. Modeling of current and temperature distributions. Mater Sci Eng A 394(1):139–148
4. Vanmeensel K, Laptev A, Vleugels J, Van der Biest O (2005) Modelling of the temperature distribution during field assisted sintering. Acta Mater 53:4379–4388
5. Gurt-Santanach J, Estournès C, Weibel A, Chevallier G, Bley V, Laurent Ch, Peigney A (2011) Influence of pulse current during spark plasma sintering evidenced on reactive alumina–hematite powders. J Eur Ceram Soc 31:2247–2254
6. Bates JL, Gamier JE (1981) Electrical conductivity of $MgAl_2O_4$ and $Y_2Al_5O_{12}$. J Am Ceram Soc 64:C138–C141
7. Chaim R (2013) Electric field effects during spark plasma sintering of ceramic nanoparticles. J Mater Sci 48:502–510. doi:10.1007/s10853-012-6764-9
8. Marder R, Estournès C, Chevallier G, Chaim R (2014) Plasma in spark plasma sintering of ceramic particle compacts. Scripta Mater 82:57–60
9. Marder R, Estournès C, Chevallier G, Chaim R (2015) Spark and plasma in spark plasma sintering of rigid ceramic nanoparticles: a model system of YAG. J Eur Ceram Soc 35:211–218
10. Zhang ZH, Wang FC, Wang L, Li SK, Shen MW, Osamu S (2008) Microstructural characteristics of large-scale ultrafine-grained copper. Mater Charac 59:329–333
11. Saunders T, Grasso S, Reece MJ (2015) Plasma formation during electric discharge (50 v) through conductive powder compacts. J Eur Ceram Soc 35:871–877
12. Zhang Z, Liu Z, Lu J, Shen X, Wang F, Wang Y (2014) The sintering mechanism in spark plasma sintering—proof of the occurrence of spark discharge. Script Mater 81:56–59
13. Saunders T, Grasso S, Reece MJ (2015) Plasma formation during electric discharge (50 V) through conductive powder compacts. J Eur Ceram Soc 35:871–877
14. Takuma T (1991) Field behavior at a triple junction in composite dielectric arrangements. IEEE Trans Dielectr Electr Insul 26:500–509
15. Takuma T, Kawamoto T, Fujinami H (1982) Effect of conduction on field behavior near singular points in composite medium arrangements. IEEE Trans Dielectr Electr Insul El-17 3:269–275

16. Tokita M (1993) Trends in advanced SPS spark plasma sintering systems and technology. J Powder Technol Japan 30:790–804
17. Meyer S, Song C, Jin Y, Wang K, Makse H (2010) Jamming in two-dimensional packings. Phys A 389:5137–5144
18. Soille P (1994) Generalized geodesy via geodesic time. Pattern Recogn Lett 15:1235–1240
19. Pavia A, Durand L, Ajustron F, Bley V, Chevallier G, Peigney A, Estournès C (2013) Electro-thermal measurements and finite element method simulations of a spark plasma sintering device. J Mater Process Tech 213:1327–1336
20. Molénat G, Durand L, Galy J, Couret A (2010) Temperature control in spark plasma sintering: an FEM approach. J Metal 2010:1–9
21. Ye Y, Li X, Hu K, Lai Y, Li Y (2013) The influence of premolding load on the electrical behavior in the initial stage of electric current activated sintering of carbonyl iron powders. J Appl Phys 113:214902
22. Timsit RS (1999) Electrical contact resistance: properties of stationary interfaces. IEEE Trans Compon Packag Technol 22:85–98
23. German RM (2014) Coordination number changes during powder densification. Powder Technol 253:368–376
24. Anselmi-Tamburini U, Gennari S, Garay JE, Munir ZA (2005) Fundamental investigations on the spark plasma sintering/synthesis process. Mater Sci Eng A 394:139–148
25. Chaim R (2007) Densification mechanisms in spark plasma sintering of nanocrystalline ceramics. Mater Sci Eng, A 443:25–32
26. Lekner J (2011) Capacitance coefficients of two spheres. J Electrostat 69:11–14